

## Article

# Effects of Mineral Composition on Movable Fluid Porosity in Micro-Nanoscale Porous Media

Quanqi Dai <sup>1,2,\*</sup>, Yangwen Zhu <sup>1,2</sup>, Yingfu He <sup>1,2</sup>, Rui Wang <sup>1,2</sup>, Da Zheng <sup>3</sup>, Yinbang Zhou <sup>1,2</sup>, Yunfeng Liu <sup>1,2</sup>, Guiwen Wang <sup>4</sup> and Hao Wu <sup>5</sup>

<sup>1</sup> State Key Laboratory of Shale Oil and Gas Enrichment Mechanisms and Effective Development, Beijing 102206, China

<sup>2</sup> Petroleum Exploration and Development Research Institute, SINOPEC, Beijing 102206, China

<sup>3</sup> Research Institute of Petroleum Exploration and Development, PetroChina, Beijing 100083, China

<sup>4</sup> College of Geosciences, China University of Petroleum—Beijing, Beijing 102249, China

<sup>5</sup> School of Earth Sciences, Lanzhou University, Lanzhou 730000, China

\* Correspondence: daiqq0614@outlook.com

**Abstract:** In natural micro-nanoscale porous media, the movable fluid porosity can effectively represent storage and permeable properties, but various mineral compositions have complicated effects on it. Taking saline lacustrine shale as an example, this study researched the effects of mineral composition on movable fluid porosity, based on nuclear magnetic resonance (NMR), focused ion beam (FIB), and x-ray diffraction (XRD) experiments. The results show that movable fluid porosity exhibits a stronger dependence on porosity than movable fluid saturation does. Micropores (<100 nm) and macropores (>1000 nm) are mostly developed in silicate and gypsum minerals, and have a highly heterogeneous distribution. In contrast, carbonate intercrystalline pores are dominated by mesopores (100–1000 nm), and behave strongly heterogeneously. Many mesopores play a positive role in generating highly movable fluid porosity, but the development of micropores and macropores is not conducive to an increase in movable fluid porosity. Overall, a significant negative effect is observed between silicate mineral content and movable fluid porosity, and carbonate mineral content has a strong positive effect on movable fluid porosity, whereas movable fluid porosity exhibits a relatively small reduction with an increase in the gypsum.

**Keywords:** micro-nanoscale porous media; movable fluid porosity; mineral composition; saline lacustrine; shale



**Citation:** Dai, Q.; Zhu, Y.; He, Y.; Wang, R.; Zheng, D.; Zhou, Y.; Liu, Y.; Wang, G.; Wu, H. Effects of Mineral Composition on Movable Fluid Porosity in Micro-Nanoscale Porous Media. *Energies* **2023**, *16*, 5166. <https://doi.org/10.3390/en16135166>

Academic Editors: Xiaoqiong Wang, Shan Wu, Mianmo Meng and Junrong Liu

Received: 10 April 2023

Revised: 29 June 2023

Accepted: 30 June 2023

Published: 5 July 2023



**Copyright:** © 2023 by the authors. Licensee MDPI, Basel, Switzerland. This article is an open access article distributed under the terms and conditions of the Creative Commons Attribution (CC BY) license (<https://creativecommons.org/licenses/by/4.0/>).

## 1. Introduction

The movable fluid porosity can reflect the volumetric fraction of movable fluid in the total pore space, and also directly indicate the amount of crude oil and gas that can be recovered [1–3]. In oil and gas reservoirs, according to the production strategy for water driving gas, the movable fluid porosity can be used to predict the movable volume of free oil at pore scale [2–4]. The movable fluid porosity can also provide a realistic assessment of the amount of oil that can flow in the porous media [3,5]. Overall, it is of great importance to quantitatively study the movable fluid porosity, to propose proper strategies to explore and develop oil and gas reservoirs [6–9].

As the global demand for oil and gas continues to increase, the exploration and development of unconventional oil and gas will become more and more important [5,10–12]. Unconventional oil and gas reservoirs are generally micro-nanoscale porous media, which are characterized by poor physical properties [12–14]. Meanwhile, unconventional oil and gas reservoirs have various mineral compositions. Due to the different types of pore that tend to develop in different minerals, unconventional oil and gas reservoirs have a complex pore-throat connectivity, and strong heterogeneity [10,13]. Previous studies have found that the development of clay minerals generally reduces the movable fluid porosity [3,7],

but other minerals have differential effects on the movable fluid porosity. Meanwhile, the mineral composition not only affects the movable fluid porosity, but also affects the recovery of valuable elements [15,16]. Overall, it is very necessary to be clear about the contributions of various minerals to the movable fluid porosity.

Recently, the Yingxi area has been the subject of increasing focus, because of the discovery of hydrocarbons in the upper of the Lower Ganchaigou Formation ( $E_3^2$ ) shale reservoirs [17,18]. The Yingxi area is located at the northwestern margin of the Yingxiongling tectonic belt, in the western Qaidam Basin, China. With the lifting of the Qinghai–Tibet Plateau, the basin seal, a cold dry climate, and plenty of salt, the  $E_3^2$  shales of the Yingxi area have developed typical saline lacustrine shales since the Cenozoic era [19]. The  $E_3^2$  shales belong to deep lake and semi-deep saline lacustrine sedimentary environments, which are characterized by tight physical properties and frequent interbedded layers [17,19]. Meanwhile, the saline lacustrine sedimentary background also results in the  $E_3^2$  shales being characterized by various mineral compositions [20,21]. In this study, the aim is to research the effects of the mineral composition on the movable fluid porosity in the micro-nanoscale porous media on the basis of  $E_3^2$  saline lacustrine shales.

## 2. Experimental Samples and Methods

In this study, a collection of core plug samples of the  $E_3^2$  shale reservoirs was taken from seven petroleum exploration wells drilled in the Yingxi area. The 35 standard core plug samples, 1 inch long and 2.0 inches in diameter, were firstly used for a nuclear magnetic resonance (NMR) experiment, and then the 35 samples were tested using x-ray diffraction (XRD) and scanning electron microscope (SEM) experiments. According to the characteristics of their mineral composition, three typical samples were selected to be tested by the focused ion beam (FIB) experiment.

The NMR experiments were conducted at the State Key Laboratory of Shale Oil and Gas Enrichment Mechanisms and Effective Development in China. The NMR apparatus required 6000 ms to echo every  $T_e$  0.2 ms, and the signal superposition was 128 times in a turnaround time. Before the NMR experiment, the core plug samples were saturated with water for 24 h under the pressure of 20 MPa, and then, in this state, the saturated  $T_2$  spectrum was obtained. In addition, a centrifugal force of 5.52 MPa was used to remove the movable water from the saturated core plug samples for 120 min, and then these core plug samples were tested, to obtain the centrifugal  $T_2$  spectra.

After the NMR experiments, part of every sample was powdered to less than 5  $\mu\text{m}$ , and oven-dried at 90 °C for 12 h, and then was XRD tested [7]. The SEM experiments were used to identify the pore-throat characteristics. Based on the above results, three typical samples were selected from the above 35 samples, to be tested using the FIB experiment, with an accuracy of 10 nm. The maximum sphere algorithm was used to extract the pore-to-throat network models corresponding to the pore space topology of real cores, and the results were composed of the pore radius and throat radius.

## 3. Results

### 3.1. Movable Fluid Porosity

As shown in Table 1, the porosities range from 0.65% to 12.03%, and the average value is 6.46%. Among the movable fluid saturations, although the maximum value is 68.89%, the minimum value is only 6.27%. Meanwhile, the movable fluid porosities are between 0.27% and 5.17%, with an average value of 2.23%. Overall, the porosity, movable fluid saturation, and movable fluid porosity have large distribution ranges, indicating that the  $E_3^2$  shale reservoirs have a strong heterogeneity.

Due to the movable fluid porosity being the multiplication of the porosity and the movable fluid saturation, the porosity and movable fluid saturation are the direct factors of the movable fluid porosity [2,3]. Figure 1 shows that the porosity increases with an increase in the porosity or movable fluid saturation, but the porosity and movable fluid saturation can have different levels of influence on the movable fluid porosity. The movable fluid

porosity shows a stronger correlation with the porosity than the movable fluid saturation does. Among the  $E_3^2$  shales, the porosity plays a more decisive role in controlling the movable fluid porosity, compared with the movable fluid saturation.

**Table 1.** Correlation statistics of the mineral and physical properties of  $E_3^2$  formations in the Yingxi area.

Type		Maximum/%	Minimum/%	Average/%
Physical property	porosity	12.03	0.65	6.46
	movable fluid saturation	68.89	6.27	35.74
	movable fluid porosity	5.17	0.27	2.23
Mineral composition	dolomite	52.6	12.5	34.8
	calcite	15.7	4.3	9.4
	carbonate	64.1	19.5	44.2
	quartz	32.6	10.7	16.2
	feldspar	15.8	2.9	4.4
	clay	46.2	15.5	28.3
	silicate	72.7	31.4	48.9
	gypsum	8.7	2.1	3.8

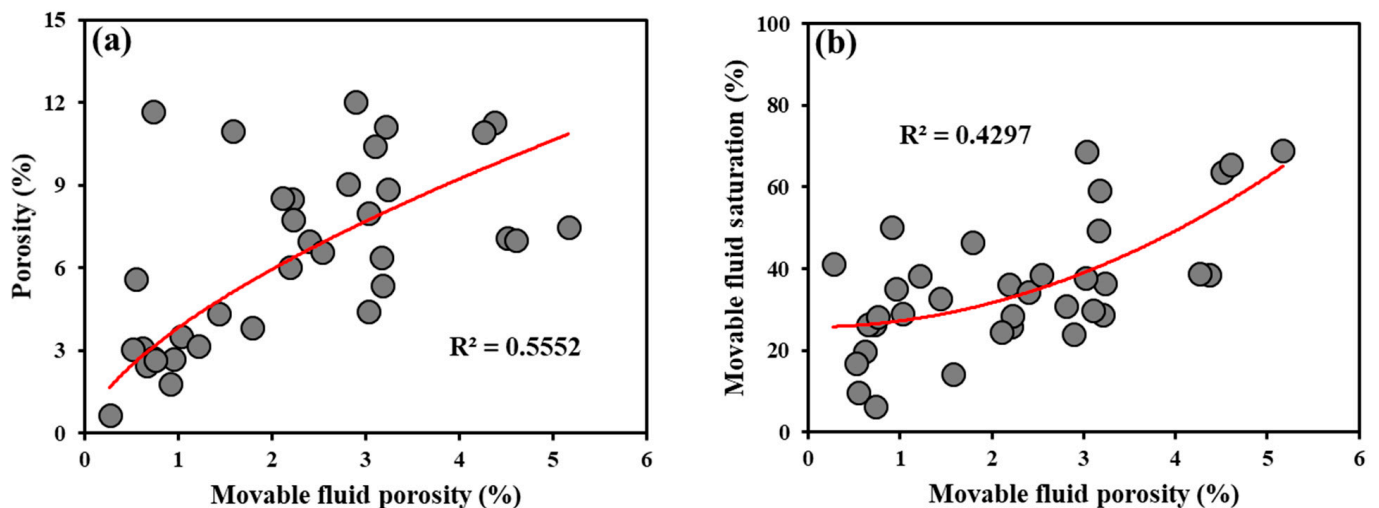


**Figure 1.** (a) Relationship between movable fluid porosity and porosity; (b) relationship between movable fluid porosity and movable fluid saturation. Note: red line, correlation curve; circle, data point.

### 3.2. Mineral Composition

The main mineral types of the  $E_3^2$  shales are dolomite, calcite, quartz, feldspar, illite, chlorite, kaolinite, gypsum, and pyrite. The contents of the different minerals are quite variable (Table 1). For the purposes of this study, the mineral compositions are divided into (1) the carbonate group (dolomite and calcite), (2) the silicate group (quartz, feldspar, and clay), and (3) gypsum. Among the mineral groups, the carbonate group accounts for 19.5% to 64.1%, the silicate group ranges between 31.4% and 72.7%, and the gypsum has the lowest proportion, ranging from 2.1% to 8.7% (Table 1). Meanwhile, the clay mineral accounts for the highest proportion of the silicate group, and the dolomite mineral contributes the most to the carbonate group. Overall, the  $E_3^2$  shales are characterized by various mineral compositions, and dominated by carbonate and silicate minerals.

### 3.3. Pore Types

According to pore size, pore types can be divided into micropores (<100 nm), mesopores (100–1000 nm), and macropores (>1000 nm) [4,14,22]. The micropores are known as

adsorption pores, and the mesopores and macropores are referred to as seepage pores [23]. In the core NMR experiment, the micropores are generally saturated with irreducible fluids that cannot be expelled using centrifugation, and the mesopores and macropores are saturated with movable fluids that can be partially expelled using centrifugation [5,14]. Meanwhile, due to the transverse relaxation time ( $T_2$ ) of the core NMR experiment having a good correspondence with the pore size [3,5], the pore types of the  $E_3^2$  shales can be identified as follows: micropore (<1 ms, <100 nm), mesopore (1–30 ms, 100–1000 nm), and macropore (>30 ms, >1000 nm). Figure 2 shows that the pore-size distributions of the different  $E_3^2$  shale samples vary greatly. Most of the samples are dominated by numerous mesopores, and some of the samples are characterized by micropores and mesopores, whereas only a small number of samples have a medium percentage of macropores (Figure 2).

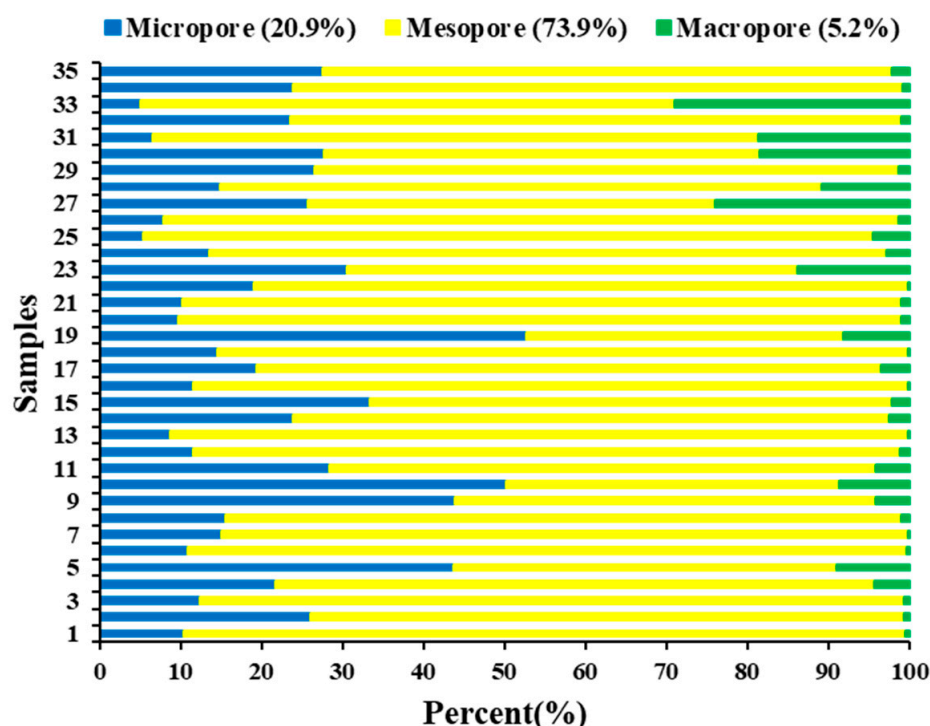
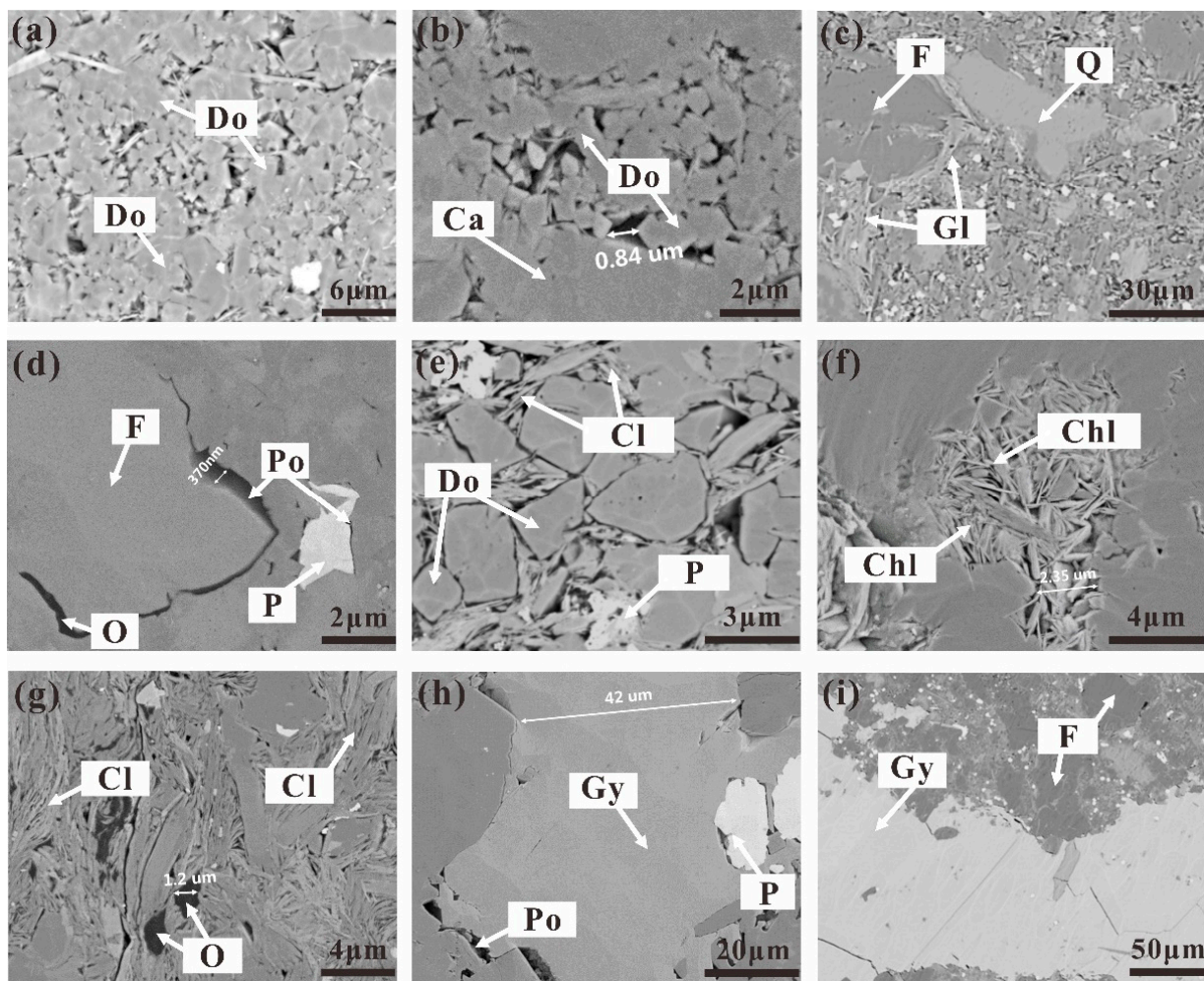
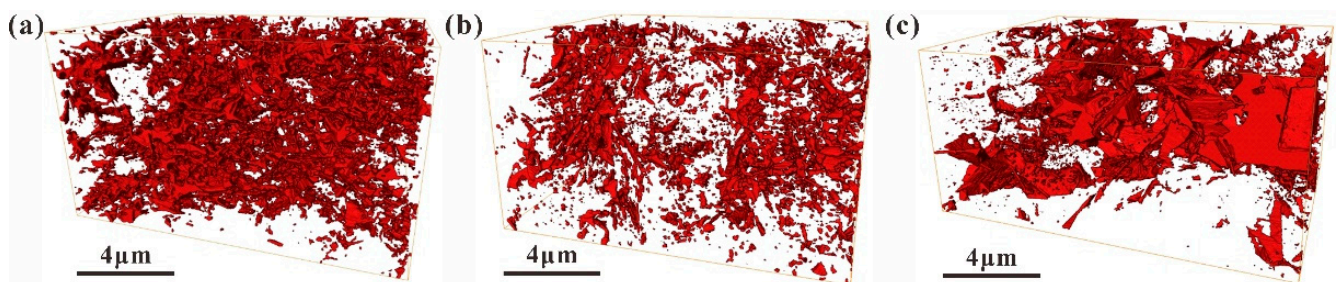


Figure 2. The percentages of different types of pore in  $E_3^2$  shales in the Yingxi area.

As shown in Figure 3, plenty of intercrystalline pores with submicron radii are developed in the carbonate minerals (Figure 3a,b), and the carbonate intercrystalline pores show a relatively homogeneous distribution in the 3D space (Figure 4a). The quartz and feldspar particles are tightly surrounded by the mineral crystals of dolomite and glauberite, resulting in the pore radii being mostly nanoscale (Figure 3c,d). Compared with the carbonate intercrystalline pores, the number and size of the silicate mineral pores are greatly reduced in the 3D space (Figure 4a,b). In addition, many clay minerals contain abundant nanoscale pores, which are formed by further filling the spaces in carbonate intercrystalline pores and silicate interparticle–intercrystalline pores (Figure 3e–g). It should be noticed that the radii of gypsum intergranular pores are submicron- or micron-sized (Figure 3h), which is highly heterogeneous in the 3D space (Figure 4c). Meanwhile, only some of the gypsum minerals are surrounded by fine grains and muddy impurities, resulting in the poor development of pores (Figure 3i). Overall, the pore types and sizes of various minerals in  $E_3^2$  shales are very different.



**Figure 3.** Microcosmic pore structure of the  $E_3^2$  typical shale samples, (a) carbonate intercrystalline pores; (b) carbonate intercrystalline pores; (c) silicate minerals; (d) feldspar interparticle pores; (e) clay mineral intercrystalline pores; (f) chlorite mineral intercrystalline pores; (g) clay minerals; (h) gypsum interparticle pores; (i) gypsum mineral. Note: Po, pore; Do, dolomite; Ca, carbonate; F, feldspar; Q, quartz; P, pyrite; O, organic; Cl, clay; Chl, chlorite; Gy, gypsum.



**Figure 4.** Characteristics of the 3D pore network: (a) all pores mainly developed in the carbonate group; (b) all pores mainly developed in the silicate group; (c) all pores mainly developed in gypsum.

Figure 5 shows the relationships between the pore types and mineral compositions. Among the mineral groups, the cumulative percentages of micropores and mesopores increase with the increasing mineral content for the silicate group and carbonate group, respectively (Figure 5a,b). As the gypsum increases, the macropores actually show a significant increase (Figure 5c). Overall, it can be found that specific mineral groups in the  $E_3^2$  shale have relatively concentrated pore-size distributions. The carbonate intercrystalline

pores are dominated by mesopores, and the silicate interparticle–intercrystalline pores are mainly micropores, whereas macropores dominate in the gypsum intergranular pores.

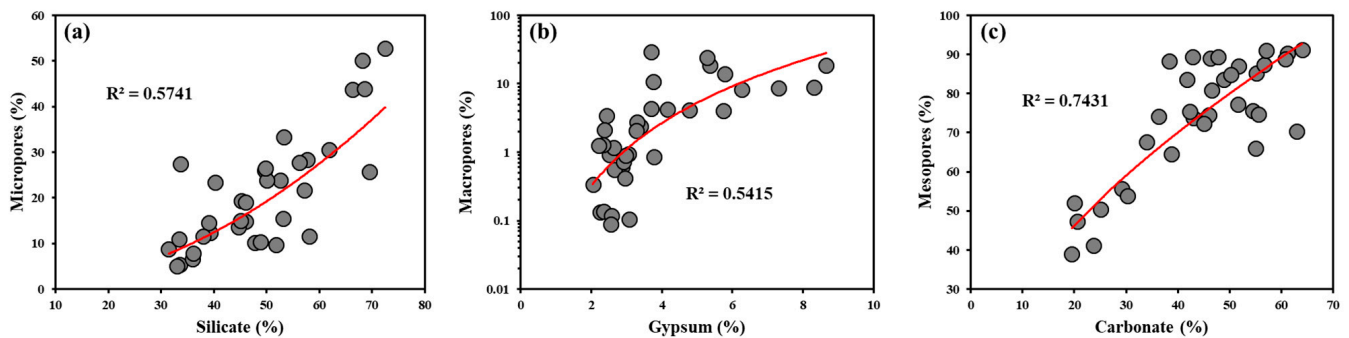


**Figure 5.** Relationships between different types of minerals and pores: (a) the silicate mineral group and micropores; (b) gypsum and macropores; (c) the carbonate mineral group and mesopores. Note: red line, correlation curve; circle, data point.

#### 4. Discussions

##### 4.1. Relationships between Porosity and Pore Types

The porosity can effectively reflect the shale reservoir capacity (Dai et al., 2021 [5]). As shown in Figure 6, there are nonlinear relationships between the porosity and the cumulative percentages of different pores, and the different types of pore offer various contributions to the porosity in the  $E_3^2$  shales. The development of mesopores is beneficial to an increase in porosity, while the increase in micropores and macropores causes a decrease in porosity (Figure 6). Among the three types of pore, the mesopores have the strongest influence on the porosity, with a correlation index of 0.6176 (Figure 6b). In the  $E_3^2$  shales, the mesopores are composed of carbonate intercrystalline pores (Figure 3a,b), and carbonate minerals have the highest percentage among the mineral composition (Table 1). Meanwhile, the quantitative advantage of the carbonate intercrystalline pores can make up for the defect of their relatively small radius, to provide enough spaces (Figures 3a,b and 4a). Thus, the porosity increases with an increase in the mesopores.

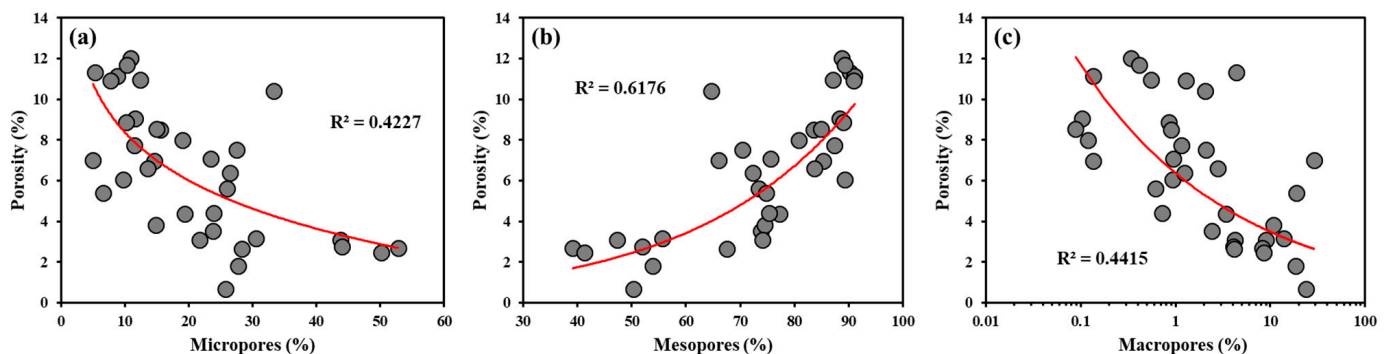


**Figure 6.** Relationships between the different types of pore and the porosity: (a) micropores and porosity; (b) mesopores and porosity; (c) macropores and porosity. Note: red line, correlation curve; circle, data point.

As illustrated in Figure 6a, the porosity generally decreases as the micropores increase, with a correlation index of 0.4227. The same negative correlation between porosity and micropores is also found in the other sedimentary basins [24,25]. In the  $E_3^2$  shales, this phenomenon occurs mainly because more micropores are associated with a higher-silicate mineral group (Figure 5a). Regarding the clay of the silicate mineral group, its deformability during the compaction process easily leads to a reduction in the number and radii of pores [7,26], and the primary pores are mostly filled with fine-clay impurities, resulting

in a reduction in the pore space (Figure 3e–g). Meanwhile, the quartz and feldspar of the silicate mineral group always have a large particle size and low structure order degree, and are tightly surrounded by dolomite crystals in the  $E_3^2$  shale reservoirs (Figure 3c,d). These phenomena can all cause the porosity to decrease with an increase in micropores.

Previous studies discovered that macropores showed a positive correlation with porosity [2,7,14]. However, Figure 6c shows that macropores exert a negative influence on porosity. In the  $E_3^2$  shale reservoirs, macropores are mainly composed of gypsum intergranular pores, and increase with an increase in gypsum (Figure 5b). Meanwhile, Figure 3 shows that the gypsum grains mostly have widths greater than 40  $\mu\text{m}$ , which are generally larger than those of other mineral grains. The higher the grain radius, the lower the surface porosity [14,27]. Therefore, a higher number of macropores always leads to a lower surface porosity, and then results in a lower porosity in the  $E_3^2$  shale reservoirs.

#### 4.2. Relationships between Movable Fluid Saturation and Pore Sizes

Movable fluid saturation is a key parameter in evaluating the moveable fluid space in shale reservoirs [1,4]. In the NMR experiment, the core  $T_2$  geometric mean value corresponds well to the average pore size [2,5,28]. As shown in Figure 7, there is a good positive correlation between the movable fluid saturation and the  $T_2$  geometric mean value, indicating that the average pore size is a main control factor in the movable fluid saturation in the  $E_3^2$  shale reservoirs. Meanwhile, the cumulative percentage differences of the various types of pore directly affect the average pore size in the  $E_3^2$  shale reservoirs (Figure 8). As the  $T_2$  geometric mean values increase, the micropores decrease (Figure 8a), whereas the mesopores increase (Figure 8b). In contrast, the  $T_2$  geometric mean values only increase with an increase in some of the macropores, indicating that not all of the macropores have a positive influence on the  $T_2$  geometric mean value (Figure 8c). This is because when the macropores increase, the macropore percentage of many cores is still much lower than the percentage of micropores or mesopores (Figure 2). The influence of macropores on the  $T_2$  geometric mean value still depends on the cumulative percentages of the micropores and mesopores.

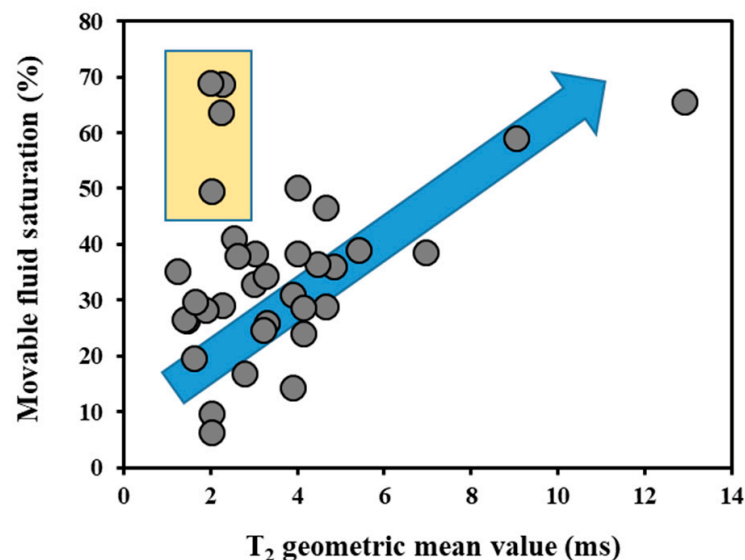


**Figure 7.** Relationships between the movable fluid saturation and the  $T_2$  geometric mean value. Note: arrow, trend line; circle, data point; block, data points of macropores.

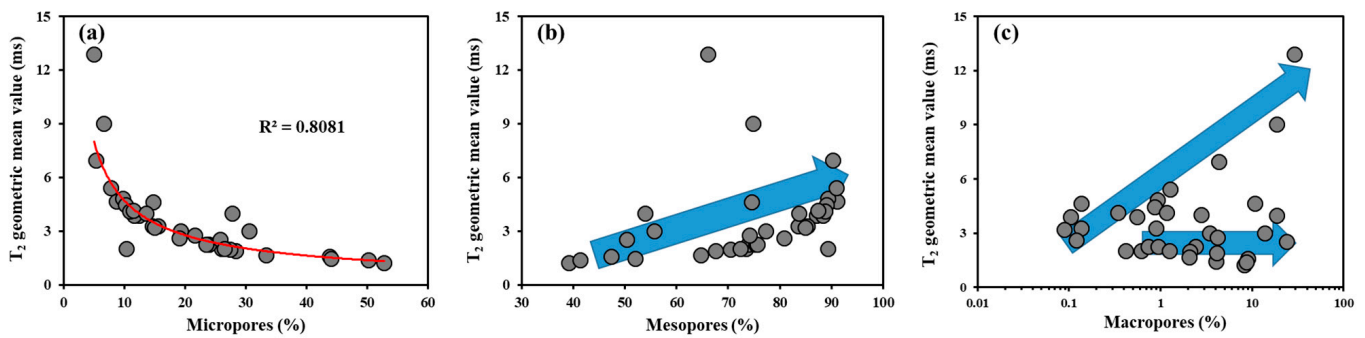


**Figure 8.** Relationships between different types of pore and the  $T_2$  geometric mean value: (a) micropores and the  $T_2$  geometric mean value; (b) mesopores and the  $T_2$  geometric mean value; (c) macropores and the  $T_2$  geometric mean value. Note: red line, correlation curve; arrow, trend line; circle, data point.

In the  $E_3^2$  shale reservoirs, the increase in micropores leads the average pore size to decrease (Figure 8a), resulting in a higher percentage of irreducible fluid space. In contrast, the movable fluid space converges to a higher value with an increase in mesopores, which is because mesopores mainly have a large average pore size (Figure 8b). Thus, an increase in micropores is not conducive to an increase in movable fluid saturation, and an increase in mesopores has a positive influence on the increase in the movable fluid saturation. On the other hand, only when the percentage of macropores is very high, does it have an absolute positive influence on the  $T_2$  geometric mean value (Figure 8c). Thus, an increase in the macropores does not completely increase the movable fluid saturation in the  $E_3^2$  shale reservoirs.

#### 4.3. Effects of Mineral Composition on Movable Fluid Porosity

In shale reservoirs, the content of various minerals is one of the most important factors for evaluating the movable fluid porosity. Figure 9 shows the effects of different mineral groups on the movable fluid porosity in the  $E_3^2$  shale reservoirs. There is a significant negative correlation between the silicate mineral group and the movable fluid porosity (Figure 9a). This is because the micropore is very sensitive to the silicate mineral group (Figure 5a). Micropores increase when the percentage of the silicate mineral group increases (Figure 5a), resulting in a decrease in porosity (Figure 6a). Meanwhile, due to the movable fluid saturation decreasing with the increase in micropores (Figure 8a), the silicate mineral group is not conducive to movable fluid saturation. Therefore, the development of silicate minerals decreases the movable fluid porosity in the  $E_3^2$  shale reservoirs.

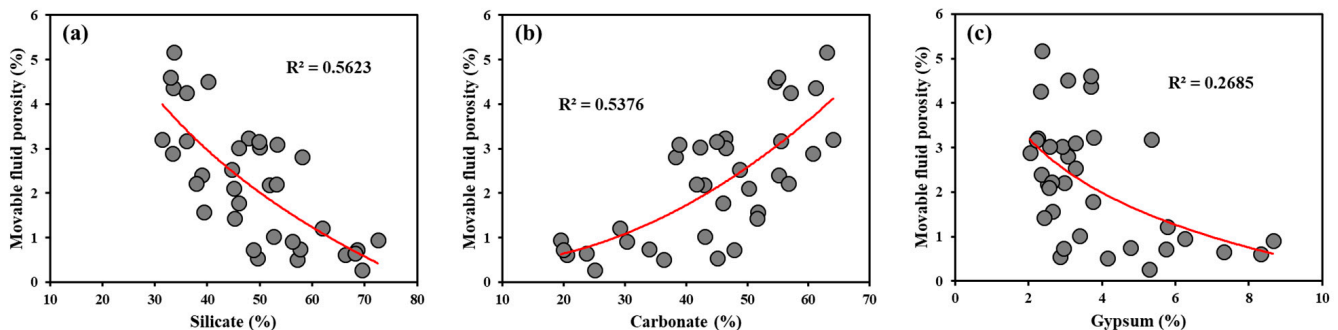


**Figure 9.** Relationships between different types of mineral and movable fluid porosity: (a) the silicate group and movable fluid porosity; (b) the carbonate group and movable fluid porosity; (c) gypsum and movable fluid porosity. Note: red line, correlation curve; circle, data point.

In the  $E_3^2$  shale reservoirs, the carbonate mineral group plays an important role in evaluating the movable fluid porosity, because of its extensive development. As shown in

Figure 8, the carbonate mineral group demonstrates a strong positive correlation with the movable fluid porosity (Figure 8b). It is mentioned in Section 3.3 that the intercrystalline pores developed in the carbonate minerals are mostly mesopores (Figure 3), which can effectively provide sufficient reservoir porosity (Figure 6b). This is one of the reasons why the movable fluid porosity increases with an increase in the carbonate mineral group. On the other hand, a large number of intercrystalline pores developed in carbonate minerals are mostly seepage pores, which have a relatively homogeneous distribution in the 3D space (Figure 4a), and when the number of carbonate intercrystalline pores increases, the average pore size increases (Figure 8b). Accordingly, the development of the carbonate mineral group is conducive to an increase in the movable fluid saturation. This is another reason why carbonate minerals have a positive effect on the movable fluid porosity.

Though gypsum is an endemic mineral to the  $E_3^2$  shale reservoir, it is also a relatively minor component in the total minerals (Table 1). Compared with the silicate and carbonate mineral groups, the correlation index between gypsum and the movable fluid porosity decreases to 0.2685 (Figure 9c). As shown in Figures 3 and 4, macropores are mostly developed in the gypsum mineral, but much of the gypsum mineral is generally tightly surrounded by fine grains and muddy impurities, resulting in the gypsum intergranular pores being highly heterogeneous in the 3D space. Accordingly, many of the macropores developed in the gypsum mineral, which are referred to as the seepage space, are restricted by the tiny pore throats. This phenomenon leads to the gypsum mineral having a relatively positive effect on the movable fluid saturation, as mentioned in Section 4.2. Meanwhile, the porosity decreases with an increase in the gypsum mineral (Figure 6c), and the movable fluid porosity has a stronger dependence on the porosity than the movable fluid saturation does (Figure 1). Therefore, the movable fluid porosity shows a relatively small reduction with the development of gypsum, compared with the development of silicate and carbonate minerals.

## 5. Conclusions

Regarding the  $E_3^2$  saline lacustrine shales, a typical micro-nanoscale porous medium, three main conclusions can be drawn, as follows.

- (a) Three pore types can be identified by the  $T_2$  spectrum: micropores (<1 ms, <100 nm), mesopores (1–30 ms, 100–1000 nm), and macropores (>30 ms, >1000 nm). The mineral compositions are divided into the carbonate group (dolomite and calcite), the silicate group (quartz, feldspar, and clay), and gypsum. Among them, micropores and macropores increase relative to the silicate mineral group and gypsum increasing, respectively, whereas a strong positive correlation is observed between mesopores and the carbonate mineral group.
- (b) An increase in mesopores makes a significant contribution to the increase in porosity and movable fluid saturation, whereas the developments of micropores are not conducive to the increase in porosity and movable fluid saturation. The macropores have a negative effect on the increase in porosity, and only a high percentage of them will completely increase the movable fluid saturation.
- (c) Various minerals lead to complicated effects on the movable fluid porosity. The carbonate mineral group has a strong positive effect on the movable fluid porosity, and a significant negative effect is observed between the silicate mineral group and the movable fluid porosity, whereas the movable fluid porosity increases slightly with an increase in gypsum.

**Author Contributions:** Methodology, Q.D. and Y.Z. (Yinbang Zhou); Software, D.Z.; Investigation, Y.Z. (Yinbang Zhou); Data curation, Q.D. and Y.L.; Writing—original draft, Q.D.; Writing—review & editing, Q.D., Y.Z. (Yangwen Zhu), Y.H., R.W., G.W. and H.W.; Supervision, G.W.; Funding acquisition, Q.D. and G.W. All authors have read and agreed to the published version of the manuscript.

**Funding:** This work was financially supported by the project funded by China Postdoctoral Science Foundation (2022M723499), the project of the Science and Technology Department of Sinopec (P21075-1, P21075-2, P22213-4), and the National Natural Science Foundation of China (41872133).

**Data Availability Statement:** No new data were created or analyzed in this study. Data sharing is not applicable to this article.

**Acknowledgments:** We are indebted to the editors and the reviewers for their constructive comments, which improved the paper significantly.

**Conflicts of Interest:** The authors declare no conflict of interest.

## References

1. Dai, Q.Q.; Wang, G.W.; Lu, C.J.; Zhang, Y.Z.; Fan, X.Q.; Wang, S.; He, Z.B. Occurrence characteristics and controls over mobile fluids in a tight sandstone reservoir. *Aust. J. Earth Sci.* **2018**, *65*, 877–887. [[CrossRef](#)]
2. Gao, H.; Li, H.Z. Determination of movable fluid percentage and movable fluid porosity in ultra-low permeability sandstone using nuclear magnetic resonance (NMR) technique. *J. Petrol. Sci. Eng.* **2015**, *133*, 258–267. [[CrossRef](#)]
3. Dai, Q.Q.; Luo, Q.; Zhang, C.; Lu, C.J.; Zhang, Y.Z.; Lu, S.J.; Zhao, Y. Pore structure of tight sandstone oil reservoir based on new parameter from NMR: Evidences from Chang 7 Member in Ordos Basin, China. *Acta Pet. Sin.* **2016**, *37*, 887–897.
4. Ouyang, Z.Q.; Liu, D.M.; Cai, Y.D.; Yao, Y.B. Investigating the fractal characteristics of pore-fractures in bituminous coals and anthracites through fluid flow behavior. *Energy Fuel.* **2016**, *30*, 10348–10357. [[CrossRef](#)]
5. Dai, Q.Q.; Wang, G.W.; Zhao, X.; Han, Z.Y.; Lu, K.; Lai, J.; Wang, S.; Li, D.; Li, Y.F.; Wu, K.Y. Fractal model for permeability estimation in low-permeable porous media with variable pore sizes and unevenly adsorbed water lay. *Mar. Pet. Geol.* **2021**, *130*, 105135. [[CrossRef](#)]
6. Gundogar, A.S.; Ross, C.M.; Akin, S.; Kovscka, A.R. Multiscale pore structure characterization of middle east carbonates. *J. Petrol. Sci. Eng.* **2016**, *146*, 570–583. [[CrossRef](#)]
7. Furmann, A.; Mastalerz, M.; Bish, D.; Schimmelmann, A.; Pedersen, P. Porosity and pore size distribution in mudrocks from the Belle Fourche and Second White Specks Formations in Alberta, Canada. *AAPG Bull.* **2016**, *100*, 1265–1288. [[CrossRef](#)]
8. Bernabéu, Á.P.; Webster, J.M.; Beaman, R.J.; Reimerd, J.P.; Renemae, W. Filling the gap: A 60 ky record of mixed carbonate-siliciclastic turbidite deposition from the Great Barrier Reef. *Mar. Pet. Geol.* **2014**, *50*, 40–50. [[CrossRef](#)]
9. Coffey, B.P.; Sunde, R.F. Lithology-based sequence-stratigraphic framework of a mixed carbonate-siliciclastic succession, Lower Cretaceous, Atlantic coastal plain. *AAPG Bull.* **2014**, *98*, 1599–1630. [[CrossRef](#)]
10. Cui, J.F.; Cheng, L. A theoretical study of the occurrence state of shale oil based on the pore sizes of mixed Gaussian distribution. *Fuel* **2017**, *206*, 564–571. [[CrossRef](#)]
11. Clarkson, C.R.; Solano, N.; Bustin, R.M.; Bustin, A.M.M.; Chalmers, G.R.L.; He, L.; Melnichenko, Y.B.; Radliński, A.P.; Blach, T.P. Pore structure characterization of North American shale gas reservoirs using USANS/SANS, gas adsorption, and mercury intrusion. *Fuel* **2013**, *103*, 606–616. [[CrossRef](#)]
12. Wang, P.F.; Jiang, Z.X.; Ji, W.M.; Zhang, C.; Yuan, Y.; Chen, L.; Yin, L.S. Heterogeneity of intergranular, intraparticle and organic pores in Longmaxi shale in Sichuan Basin, South China: Evidence from SEM digital images and fractal and multifractal geometries. *Mar. Pet. Geol.* **2016**, *72*, 122–138. [[CrossRef](#)]
13. Meng, M.M.; Peng, J.C.; Ge, H.K.; Ji, W.M.; Li, X.M.; Wang, Q.Y. Rock fabric of lacustrine shale and its influence on residual oil distribution in the Upper Cretaceous Qingshankou Formation, Songliao Basin. *Energy Fuels.* **2023**, *37*, 7151–7160. [[CrossRef](#)]
14. Zhang, P.F.; Lu, S.F.; Li, J.Q.; Zhang, J.; Xue, H.T.; Chen, C. Comparisons of SEM, Low-Field NMR, and Mercury Intrusion Capillary Pressure in Characterization of the Pore Size Distribution of Lacustrine Shale: A Case Study on the Dongying Depression, Bohai Bay Basin, China. *Energy Fuels* **2017**, *31*, 9232–9239. [[CrossRef](#)]
15. Feng, Q.C.; Yang, W.H.; Wen, S.M.; Wang, H.; Zhao, W.J.; Han, G. Flotation of copper oxide minerals: A review. *Int. J. Min. Sci. Technol.* **2022**, *32*, 1351–1364. [[CrossRef](#)]
16. Feng, Q.C.; Wang, M.L.; Zhang, G.; Zhao, W.J.; Han, G. Enhanced adsorption of sulfide and xanthate on smithsonite surfaces by lead activation and implications for flotation intensification. *Sep. Purif. Technol.* **2023**, *307*, 122772. [[CrossRef](#)]
17. Zhang, Y.S.; Wu, K.Y.; Jiang, Y.H.; Wang, P.; Cai, F.R.; Tan, W.L.; Gao, S.F.; Xian, B.Z. Geological characteristics of deep carbonate hydrocarbon-bearing pool in the western Yingxiongling area in Qaidam Basin. *Nat. Gas. Geosci.* **2018**, *29*, 358–369.
18. Huang, C.G.; Guan, X.; Ni, X.L.; Chang, H.Y.; Zhang, S.M.; Yang, S. The characteristics and major factors controlling on the E<sub>3</sub><sup>2</sup> dolomite reservoirs in saline lacustrine basin in the Yingxi area of Qaidam Basin. *Nat. Gas. Geosci.* **2017**, *28*, 219–231.
19. Wang, J.G.; Zhang, D.W.; Yang, S.Y.; Li, X.; Shi, Y.J.; Cui, J.; Zhang, P.; Wang, Y.L.; Yi, D.H.; Chang, H.Y. Sedimentary characteristics and genesis of the salt lake with the upper member of the Lower Ganchaigou Formation from Yingxi sag, Qaidam basin. *Mar. Pet. Geol.* **2019**, *111*, 135–155. [[CrossRef](#)]
20. Korngreen, D.; Bialik, O.M. The characteristics of carbonate system recovery during a relatively dry event in a mixed carbonate/siliciclastic environment in the Pelsonian (Middle Triassic) proximal marginal marine basins: A case study from the tropical Tethyan northwest Gondwana margins. *Palaeogeogr. Palaeoclimatol. Palaeoecol.* **2015**, *440*, 793–812.

21. Loucks, R.G.; Reed, R.M.; Ruppel, S.C.; Jarvie, D.M. Morphology, genesis, and distribution of nanometer-scale pores in siliceous mudstones of the Mississippian Barnett shale. *J. Sediment. Res.* **2009**, *79*, 848–861. [[CrossRef](#)]
22. Daigle, H.; Johnson, A. Combining mercury intrusion and nuclear magnetic resonance measurements using percolation theory. *Transp. Porous Media* **2016**, *111*, 669–679. [[CrossRef](#)]
23. Cai, Y.D.; Liu, D.M.; Pan, Z.J.; Yao, Y.B.; Li, J.Q.; Qiu, Y.K. Pore structure and its impact on CH<sub>4</sub> adsorption capacity and flow capability of bituminous and subbituminous coals from Northeast China. *Fuel* **2013**, *108*, 292–302. [[CrossRef](#)]
24. Chalmers, G.R.L.; Bustin, R.M. Geological evaluation of Halfway-Doig-Montney hybrid gas shale-tight gas reservoir, northeastern British Columbia. *Mar. Pet. Geol.* **2012**, *38*, 53–72. [[CrossRef](#)]
25. Milliken, K.L.; Rudnicki, M.; Awwiller, D.A.; Zhang, T. Organic matter-hosted pore system, Marcellus Formation (Devonian), Pennsylvania. *AAPG Bull.* **2013**, *97*, 177–200. [[CrossRef](#)]
26. Wu, L.R.; Huang, C.G.; Yuan, J.Y.; Cao, Z.L.; Wan, C.Z.; Pan, X.; Zhang, S.M.; Li, A.Y. Double-porosity System of mixed sediments in Saline Lacustrine Basin and its significance to reservoir. *J. Earth Sci. Environ.* **2015**, *37*, 60–66.
27. Wang, H.L.; Liu, H.F.; Li, W.; Yang, Y.L. Multifractal characterization of tectonically deformed coal pore structure based on mercury injection technology. *Saf. Coal Mines* **2016**, *47*, 33–37.
28. Rezaee, R.; Saeedi, A.; Clennell, B. Tight gas sands permeability estimation from mercury injection capillary pressure and nuclear magnetic resonance data. *J. Petrol. Sci. Eng.* **2012**, *88–89*, 92–99. [[CrossRef](#)]

**Disclaimer/Publisher’s Note:** The statements, opinions and data contained in all publications are solely those of the individual author(s) and contributor(s) and not of MDPI and/or the editor(s). MDPI and/or the editor(s) disclaim responsibility for any injury to people or property resulting from any ideas, methods, instructions or products referred to in the content.